Fatigue behaviors and damage mechanism of a Cr-Mn-N austenitic steel

Lv, Z.; Cai, P.; Yu, Tianbo; Jin, Yi; Zhang, H.; Fu, W.; Zhai, T.

Published in:
Journal of Alloys and Compounds

Link to article, DOI:
10.1016/j.jallcom.2016.08.228

Publication date:
2017

Document Version
Peer reviewed version

Fatigue properties and damage mechanism of a Cr-Mn austenite steel

Z.Q. Lv [a,d*], P. Cai[b], T. Yu[c], Y. Jin[b], H. F. Zhang[d], T. Zhai[b], W.T. Fu[a]

[a] *State Key Laboratory of Metastable Material Science and Technology, Yanshan University, Qinhuangdao 066004, China.*

[b] *Department of Chemical and Materials Engineering, University of Kentucky, Lexington, KY 40513, USA*

[c] *Department of Wind Energy, Risø Campus, Technical University of Denmark, Roskilde, DK-4000, Denmark*

[d] *College of Mechanical Engineering, Yanshan University, Qinhuangdao 066004, China*

Abstract

The fatigue properties and the damage mechanism of a Cr-Mn austenite steel were investigated using four-point bend fatigue testing. The stress-number of cycles to failure (S-N) curve of the Cr-Mn austenite steel was measured at room temperature, at the frequency of f=20 Hz and the stress ratio of R=0.1. The fatigue strength of this Cr-Mn austenite steel was measured to be 503 MPa in the maximum stress. Multiple cracks are initiated on the sample surface after fatigue failure tests, and usually only one or two of them can lead to the final failure of the samples. Most of the cracks are initiated at the {111}<110> primary slip bands, especially within coarse grains. When a fatigue crack meets a new grain, it adapts to slip bands in this grain and hardly extends along the foregoing route in the previous grain. A crack is deflected at a grain boundary by crack plane twisting and tiling on the grain boundary plane, causing fracture steps on the fracture surface.

Key words: Fatigue strength; slip bands; crack propagation; four-point bend fatigue

1. Introduction

Cr-Mn austenite steels are potential substitutions for the common Cr-Ni austenite steels, due to lower cost from the low nickel (<5%, or Ni free) content[1,2]. Generally, austenite stainless steels are metastable, wherein martensite transformation takes place either directly or indirectly[2-6], even under low cyclic stress [4-6]. In order to enhance the stability of

* Corresponding authors. State key Laboratory of Metastable Material Science and Technology, Yanshan University, Qinhuangdao 066004, China. E-mail addresses: zqlv@ysu.edu.cn

austenite phase and keep the low-cost, nitrogen is added in the steels, which can further improve the mechanical, chemical and physical properties of these steels [7,8]. Cr-Mn-N austenite steels with high strength, ductility and toughness are considered as a group of promising structural materials and biological materials that can be used in many engineering fields. Recently, the workability, weldability, corrosion resistance and deformation behavior of these steels were extensively studied [2,7-9]; however the fatigue properties of Cr-Mn-N austenite steels were rarely reported. While in many engineering applications, fatigue is the dominant failure mechanism governing the life of a component. The fatigue performance, as one of the important mechanical indicators of materials, can be investigated using some fatigue testing methods, such as torsion stress fatigue testing, axial load fatigue testing and bending fatigue testing. The four-point bend method presents some advantages over the others, e.g., convenient sample mounting and dismounting, and simple sample geometry. Therefore, the fatigue damage developed during cyclic loading can be readily monitored and studied. Using this self-aligning four-point bend testing method, Zhai et al [10-12] have successfully investigated and characterized the fatigue properties in different Al alloys, including fatigue crack initiation and early growth, fatigue weak-link (i.e., crack initiation site) density and strength distribution, and the relation between microstructure and fatigue damage.

In this work, the four-point bend fatigue testes were performed on a Cr-Mn austenite steel to measure the S-N curve and the density and the strength distribution of fatigue weak links were then described. Furthermore, the morphology of crack surface was characterized and the behaviors of initiation and propagation of cracks were discussed.

2. Material and experimental procedure

2.1 Material and samples

The test material (18Mn18Cr0.5N steel) used in this work was melted in a vacuum induction furnace. After electroslag remelting, its chemical composition was measured to be: 0.09C, 18.70Mn, 18.51Cr, 0.48N, 0.81Si, 0.05V, 0.025P, 0.005S, 0.011Al, and balance Fe in

wt.%. After austenitized at 1473 K for 60 min and cooled by water, the specimens were cut into size of 36.5 ×10 × 4.6 mm^3 for four point bend fatigue tests. As shown in Fig. 1, an average grain size of 102 μm (including twin boundaries) can be observed. Its yield and ultimate tensile strengths were measured to be 673 and 878 MPa, respectively.

2.2 Fatigue tests

Four-point bend fatigue tests were conducted at room temperature in air, at the stress ratio of 0.1 and the frequency of 20 Hz, under stress control in a sine wave [10] on an Instron 8802 servo-hydraulic materials testing machine. The run-out number was set to be 5.5×10^6 cycles for S-N curve measurement. The maximum stress levels used in the fatigue tests were varied from 105 % to 60 % of the yield strength. The loading state of four-point specimens and the specimen geometry are shown in Fig.2. The upper surface of the specimen was subjected to tension. The sample surface was ground and mechanically polished before fatigue testing.

In order to conveniently observe the morphology of the fatigue cracks, the fatigue tests were terminated automatically when the sample deflection exceeded a predefined value, 115% of the maximum deflection amplitude.

2.3 Fatigue crack and fracture surface

The fatigue cracks were characterized by means of optical microscopy (OM), scanning electron microscopy (SEM) and electron backscatter diffraction (EBSD). SEM analyses were carried out using a Zeiss Supra-35 SEM, equipped with a field emission gun and an Oxford Instruments HKL Channel 5 EBSD system. The microscope was operated at 20 kV for both electron channeling contrast (ECC) imaging and EBSD.

Some of the fatigued specimens were broken in flexural bending by hand along the dominating crack after crack population observation. The facture surfaces, especially the crack-initiation sites, were observed in a Zeiss Supra-35 SEM.

3. Results and discussions

3.1 S-N curves and crack population

Figure 3 shows the S-N curve of the Cr-Mn austenite steel measured by four-point bend testing. The fatigue life increased with decreasing stress level, and it showed a linear relationship between the applied maximum stress and the logarithm of cycles to failure. The fatigue limit was determined to be 75% yield strength (σ_s), i.e. 503 MPa.

For those samples subjected under stress level lower than the fatigue limit, slip lines can be clearly observed on the surfaces, as shown in Fig.4(a), but no crack was found. With increasing applied stress above the fatigue limit, slip lines became broad, and eventually fatigue cracks were initiated (Fig. 4(b)). From fig.4(c), multiple cracks were observed on the surface after the fatigue tests at a stress level over the fatigue limit. Most of the cracks were initiated from the previous slip lines, especially in coarse grains.

The crack population was subsequently measured from the fatigued samples and plotted against the applied maximum cyclic stress in the Cr-Mn austenite steel. As shown in fig.5, the number of cracks increases with the increase of stress level. At those stress levels above the fatigue limit, there are usually only one or two dominant cracks that lead to the final failure of samples.

Similar to the analysis done in high strength Al alloys [13,14], the relationship of applied stress level and total numbers of fatigue cracks on the surface were represented using a Weibull distribution function for the Cr-Mn austenite steel. In this work, the fitted curve of crack population vs applied maximum stress is also shown in fig.5. The Weibull function used in this work is:

$$N = N_0(1-\exp[-k(\frac{\sigma-\sigma_0}{\sigma_0})^m]) \quad (1)$$

where N_0 is the maximum possible number of cracks per mm^2 that can be formed on the surface, and approximately equals to the crack density observed on the surface in tension

(6×10 mm^2) at the stress level close to the yield strength (σ_s), and in the present work, N_0=73/60≈1.22 mm^{-2}; *k* is a constant; m is the Weibull modulus; and σ_0 is the fatigue limit, σ_0=75% σ_s. The value of k and m could be determined by fitting the crack population vs the maximum stress level curves using the Weibull function which could be rewritten as :

$$\ln(-\ln(1-\frac{N}{N_0})) = m\ln(\frac{\sigma}{\sigma_0}-1)+\ln k \tag{2}$$

The curve in Fig. 5 could be fitted by linear regression method in a ln(-ln(1-N/N_0)) vs ln(σ/σ_0-1) plot with m as the slope, as shown in Fig.6. Only the data points of crack population at relatively higher stress levels were used in the curve fitting, since the data points close to the fatigue limit were unreliable for the linear curve fitting. The fitting parameters can be found in Fig.6.

3.2 Strength distribution of fatigue weak links

If a crack is assumed to initiate from one weak link, the crack density value is approximatively equivalent to fatigue weak link density in the steel. Although these fatigue cracks were mostly initiated from the previous slip lines, this crack density value was much smaller than that of the slip lines. In other words, most slip lines in this steel cannot form fatigue cracks. The fatigue weak link density measured in the present work could be regarded as the effective weak link density of this steel, which reflects the damage behavior of fatigue crack initiation in this steel. Consequently, it can be used to evaluate the quality of an alloy in terms of fatigue crack initiation behaviors.

As depicted in fig.7, the strength distribution of fatigue weak links could also be determined from the crack population-stress relationship, which was quantified by taking the derivative of Eq.(1) [12,14]

$$n = CN_0(\frac{km}{\sigma_0})(\frac{\sigma-\sigma_0}{\sigma_0})^{m-1}\exp[-k(\frac{\sigma-\sigma_0}{\sigma_0})^m] \tag{3}$$

where

$$N_0 = \int_0^{+\infty} n d\sigma \quad (4)$$

n is the characteristic strength distribution of fatigue weak-links in material, representing the number of newly formed cracks at a specific stress level σ, and C is a scaling constant. For a material with a better fatigue property, N_0 should be as small as possible, and the peak in the weak-link strength distribution should be as narrow and low as possible[13]. In fig.7, the peak in the weak-link strength distribution is narrow, which indicates an excellent fatigue performance of the studied Cr-Mn steel.

3.3 Crack morphology and fracture surface

Multiply crack initiation sites were observed on the sample surface after the fatigue tests, and only one or two of them leads to final failure of this sample, as shown in fig.8. The slip lines were clearly visible in the studied steel, and similar slip lines were also observed in the fatigued samples of Cu alloys and Cr-Ni austenite steels [15-18], however not in Al alloys [11-14]. The dominant crack can be regarded as a coalesced crack constituted by several cracks in different grains, which extended across the grain boundaries and twin boundaries. The morphology of a dominant crack was observed using OM and ECC imaging shown in fig.9 (a) and (b), respectively. According to the OM and ECC images, the outlines of crack and grain boundaries (including twin boundaries) were draw and shown in Fig.9(c). In order to describe conveniently, the grains related to cracks were coded in numbers.

It is obvious that the propagation direction of the dominant crack was perpendicular to the principal stress. Meanwhile, the orientation of the crack deflected when it entered into the next grain. The crack within one grain was predominantly along the slip lines. Obvious jagged crack can be found in grain 1 and grain 7, which was also found in the Cr-Ni austenite steel with high nitrogen [15].

In order to further analyze the formation mechanism of the jagged shape and the transgranular feature of the crack, SEM images of the local details in the dominant crack are

shown in fig. 10. Based on EBSD data analysis, the orientation of grain and the slip systems are also given in fig.10. The details of the crack in grain 7 are shown in Fig. 10 (a). The intersection angle of jagged cracks in this surface (between line 4 and line 5) is very close to the angle of the slip lines (between the line 1 and line 2). This indicates that the initiation of a micro-crack occurs along a slip band of the {111}• <110> slip system of this austenite steel. The crack then propagated in the sample in a jagged form as guided by local slip bands. This kind of crack is beneficial to the fatigue performance of materials and can retard the crack extension in a certain extent. When a fatigue crack enters into a new grain, it will locally align with the new slip bands in this grain and it hardly extends along the foregoing route in the previous grain. Fig.10 (b) shows the partial crack across from grain 5 to grain 6. It can be seen that the direction of crack extension deflects across the boundary between grain 5 and grain 6, because there are diverse orientations of slip bands in different grains. In some previous works the phenomenon of crack deflection was pointed out in Al alloy [19,20], although these slip bands were not observed clearly. The jagged crack in grain 6 can be seen from Fig.10 (b). From fig.10(c), the crack, crossing the boundary between the grain 4 and grain 5, extends along the previous direction for a short distance in grain 5. However there is bigger propagation resistance in this direction, and then the expanding direction shifts to the approximate direction of a group of slip bands in grain 5.

In order to further analyze the formation mechanisms of jagged shape and transgranular feature of the crack, the SEM images of the local details in the dominated crack are shown in fig. 10. Combining EBSD data analysis, the orientation of grain and slip systems were also given in fig.10. The details of the crack in grain 7 are shown in Fig. 10 (a). The intersection angle of the jagged cracks on this surface (between line 4 and line 5) was very close to the angle of the slip lines (between the line1 and line 2). This indicates that the initiation of a micro-crack occurs along a slip band of the {111}<110> slip system of this austenite steel. This kind of crack is beneficial to the fatigue performance of materials by retarding crack

propagation. The jagged cracks can be regarded as the cracks from intercrossing slip bands linking together. When a fatigue crack entered next grain, instead of extending along the foregoing route from previous grain, it preferred to propagate along a new slip bands in this grain. Fig.10 (b) shows a segment of crack propagated across the grain boundary between grain 5 to 6. It can be seen that the crack plane deflected at the grain boundary due to the difference of their slip band orientation. Previous works in the Al alloys have pointed out similar phenomenon of crack deflection [19,20]. A crystallographic model for fatigue crack propagation through grain boundaries was established and indicated the key factors (the twist and tilt angles) controlling the path and growth rate of a short crack [19]. From fig.10(c), the crack, crossing the boundary between grain 4 and grain 5, extended along the previous direction for a short distance in grain 5, then the expanding direction shifted to the approximate direction of a group of slip bands in grain 5.

Fig. 11 shows a typical fracture surface of the Cr-Mn steel after four-point bend fatigue test. Crack initiation sites, grain boundaries and fracture steps can be observed on the facture surface, and are marked using arrows in fig.11. From the previous analysis, the initiations of cracks can be related to the slip planes. Comparing with the both sides of grain boundaries (red arrows in fig. 11), the deflection of cracks is visible, in agreement with the observations on the upper surface (see fig. 10). The fracture steps observed on the fracture surface provide the proof of high resistance to crack growth, according to the crystallographic model of fracture crack growth [20]. This high resistance to crack propagation may be a main reason why only one or two dominated cracks exist on the surface, while most of them were arrested and became non-propagating cracks.

3.4 Discussion

The initiation of the fatigue cracks in Cr-Ni austenite steels, e.g. 304 and 316 steel, was mainly at twin boundaries[16], slip bands and grain boundaries [4,15] , and the fatigue limit of 316L steel was 200 MPa (grain size 35 μm) [21]. When the martensitic translation ($\gamma \rightarrow \alpha'$)

was induced by cyclic strain in a Cr-Ni austenitic steel (Fe-17Cr-13Ni), the nucleation and propagation of short cracks were found within martensite phases [5]. Fatigue cracks tend to initiate at grain and annealing twin boundaries in the twinning induced plasticity (TWIP) steels with high manganese [22]. Umezawa and Nigai [23] suggested that the addition of Mn (into Cr-Ni-N austenite steel) enhanced grain boundary cracking and provided a weak link in the grain boundary. Fig.12 shows the statistical data on the frequency of initiation sites in the present work. Obviously, most cracks initiated from the slip bands, and few cracks nucleated at the grain boundaries or twin boundaries in the 18Cr-18Mn-0.5N austenite steel. Also, in a super austenitic stainless steel (25Cr-22Ni-7.6Mo-3Mn-0.46N), the crack initiation was found at the slip bands [24]. So the addition of Mn in austenite steels is not the main factor resulting in the grain boundary cracking under cyclic stresses. For austenitic steels, the decrease of the cracks initiation from grain (twin) boundaries can effectively decrease the weak links of the steels under cyclic stresses and improve their fatigue properties.

The initiation of cracks on the slip bands is closely related to the activity of slip systems, which depend on the dislocation motion and structures in the steels under low cyclic stress. The addition of nitrogen restrained the formation of dislocation cells and promoted the planar glide of dislocation [15,24], which induced the nucleation of cracks at the slip bands. Therefore the cracks initiating sites are likely affected by N in the Cr-Mn austenite steel. The activity of slip system under low-cycle stress is also related to the strain amplitudes [25], which needs more investigations in the Cr-Mn austenite steels. For 316LN austenite steels, the nucleation of cracks takes place more frequently at grain boundaries and twins in the coarse-grained austenite (average grain size 130μm), while slip bands are preferred sites for crack nucleation in the fine-grained austenite (average grain size 43μm) [15]. However, in this experimental steel (average grain size 102 μm), the initiation of cracks are mostly from the slip bands and hardly from the grain boundaries of large grains, as shown in Fig.4 (b).

The fatigue cracks propagate mainly along the slip lines and across the boundaries and

twin boundaries in the Cr-Mn austenitic steel. The propagating traces of the fatigue cracks are shown in Fig.13. The crack propagation along a single slip band is easy, as sketched in Fig. 13(a). However, multiply slip activities in this steel were also found, as shown in Fig. 13 (b). A crack extending along the intercrossing slip bands can lead to a jagged shape, as shown in Fig.10 (a), which can hinder the extending of the crack. The grain boundaries and twin boundaries can also retard the extending of the cracks, as shown in Fig.13(c),(d) and (e). In other words, the increase of the grain boundaries and twin boundaries can enhance the resistance to the crack propagation. Although the resistance of the grain boundaries and that of the twin boundaries are not calculated in this work, the difference between them is probably related to the boundary energy and grain orientation.

For this experimental steel, few cracks initiate from grain boundaries and twin boundaries, so grain refinement will be an effective method to improve the fatigue properties. Moreover, promotion of simultaneous activities of multiply slip bands will be another good method. As indicated in Fig. 13 (d) and (e), the combined action of both twin boundaries and multiply slips can restrain the extending of cracks more effectively.

4. Conclusions

The fatigue strength of the Cr-Mn austenite steel was measured to be 503 MPa at a run-out 5.5×10^6 cycles in four-point fatigue bend. Multiple cracks were observed on the sample surface after the fatigue failure tests. At each different stress level above the fatigue limit, there were usually only one or two dominated cracks that can lead to the final failure of samples. Crack population vs. stress level curve was fitted with a Weibull distribution, from which the density (N_0=1.22 mm^{-2}) and strength distribution (n) of fatigue weak links can be obtained. Most of the cracks were initiated from the slip bands of the experimental austenite steel, especially in large grains. When a fatigue crack meets a new grain, it will adapt to the new slip bands of this grain and hardly extended along the foregoing route in the previous

grain.

Acknowledgements

This research was funded by the National Natural Science Foundation of China (Nos.51101137 and 51171161). Z.Q. Lv would like to thank Prof. X. Huang for useful discussions.

Reference

[1] R .P. R. Kumtubarao, Int. Mater. Rev 34 (1989) 69–86.

[2] P. Sahu, S.K. Shee, A.S. Hamada, L. Rovatti, T. Sahu, B. Mahato, S. Ghosh Chowdhury, D.A. Porter, L.P. Karjalainen, Acta Mater. 60 (2012) 6907–6919.

[3] S. Allain, J. P. Chateau, O. Bouaziz, S. Migot, N. Guelton, Mater. Sci. Eng. A 387–389 (2004) 158–162.

[4] I. Roth, M. Kubbeler, U. Kruup. H.J. Christ, C.P. Fritzen, Procedia Engineering 2 (2010) 941-948

[5] J. Stolarz, N. Baffie, T. Magnin, Mater. Sci. Eng. A 319–321 (2001) 521-526.

[6] A. Das, Int. J. Fatigue 70 (2015) 473–479

[7] S. T. Wang, K. Yang, Y.Y. Shan, L.F. Li, Mater. Sci. Eng. A 490 (2008) 95–104.

[8] Z.H. Wang, W.T. Fu, S.H. Sun, L. Hui, Z.Q. Lv, D.L. Zhao, Metall. Mater. Trans. A 41(4) (2010) 1025-1032.

[9] A.S. Hamada, L.P. Karjalainen, R.D.K. Misra, J. Talonen, Mater. Sci. Eng. A 559 (2013) 336–344.

[10] T. Zhai, Y.G. Xu, J.W. Martin, A.J. Wilkinson, G.A.D. Briggs, Int. J. Fatigue 21 (1999) 889–894.

[11] W. Wen, Alfonso H.W. Ngan, Y. Zhang, B. Xu, T. Zhai. Mater. Sci. Eng. A 564 (2013) 97–101.

[12] Y. Jin , P. Cai, W. Wen, H. Nagaumi , B. Xu , Y. B. Zhang , T. Zhai, Mater. Sci. Eng. A 622 (2015) 7–15.

[13] Y.B. Zhang, J.H. Xu, T. Zhai. Mater. Sci. Eng. A 527 (2010) 3639–3644.

[14] T. Zhai, Metall. Mater. Trans. A 37 (2006) 3139 – 3147.

[15] U. Lindstedt, B. Karlsson, M. Nystrom, Fatigue Fract. Engng Mater. Struct. 21(1998) 85-98

[16] P. Mu, V. Aubin, Procedia Engineering 2 (2010) 1951–1960

[17] Q.S. Pan, Q.H. Lu, L. Lu, Acta Mater. 61 (2013) 1383–1393

[18] N.L. Phung, V. Favier , N. Ranc, Int. J. Fatigue 77 (2015) 115–127.

[19] T. Zhai, A. J. Wilkinson, J. W. Martin, Acta Mater. 48 (2000) 4917–4927.

[20] T. Zhai, X.P. Jiang, J.X. Li, M.D. Garratt, G.H. Bray, Int. J. Fatigue 27 (2005) 1202–1209.

[21] S. Gueler, M. Schymura, A. Fischer, Int. J. Fatigue 75 (2015) 145–152

[22] A.S. Hamada, L.P. Karjalainen, A. Ferraiuolo, J. Gil Sevillano, F. De Las Cuevas, G. Pratolongo, M. Reis, Metall. Mater. Trans. A 41 (2010) 1102-1108

[23] O. Umezawa, K. Nagai, Metall. Mater. Trans. A 29 (1998) 809-822

[24] S. Heino, B. Karlsson, Acta mater. 49 (2001) 353–363

[25] A. Das, Metall. Mater. Trans. A 45 (2014) 2927-2930

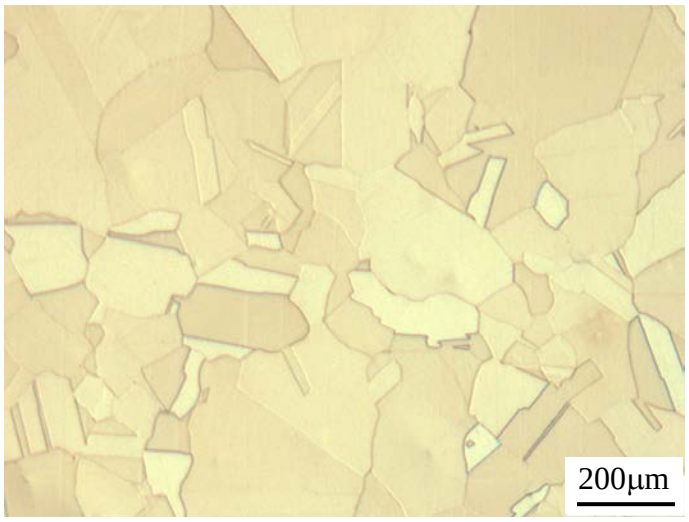

Fig.1 Microstructure of the Cr-Mn austenite steel

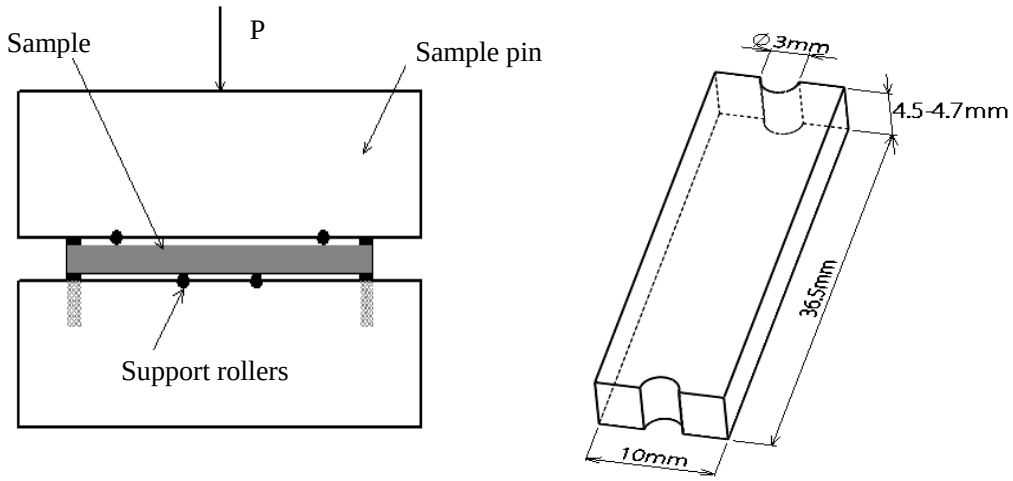

Fig.2 The setup of four-point bend testing and, and the geometry and dimensions of a four-point bend sample.

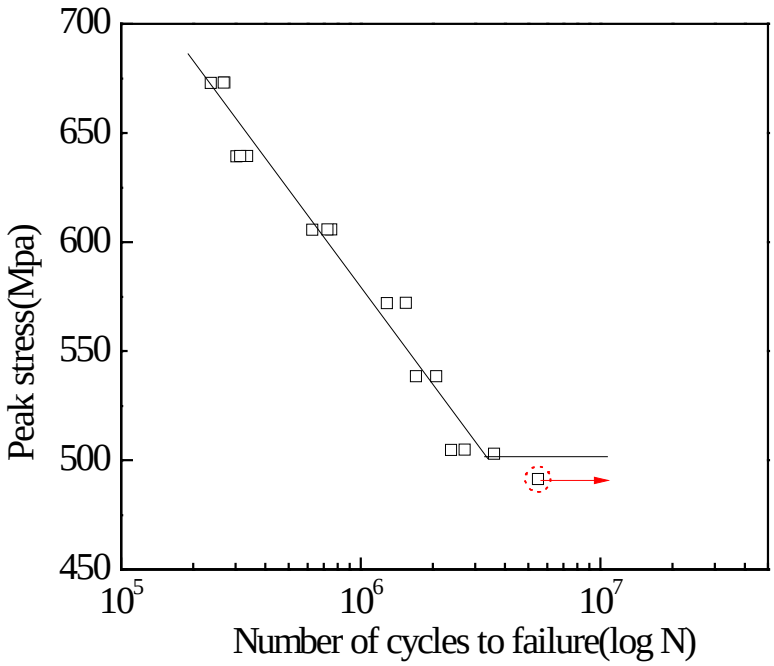

Fig 3.S-N curves of the samples of the Cr-Mn austenite steel by four-point bend fatigue

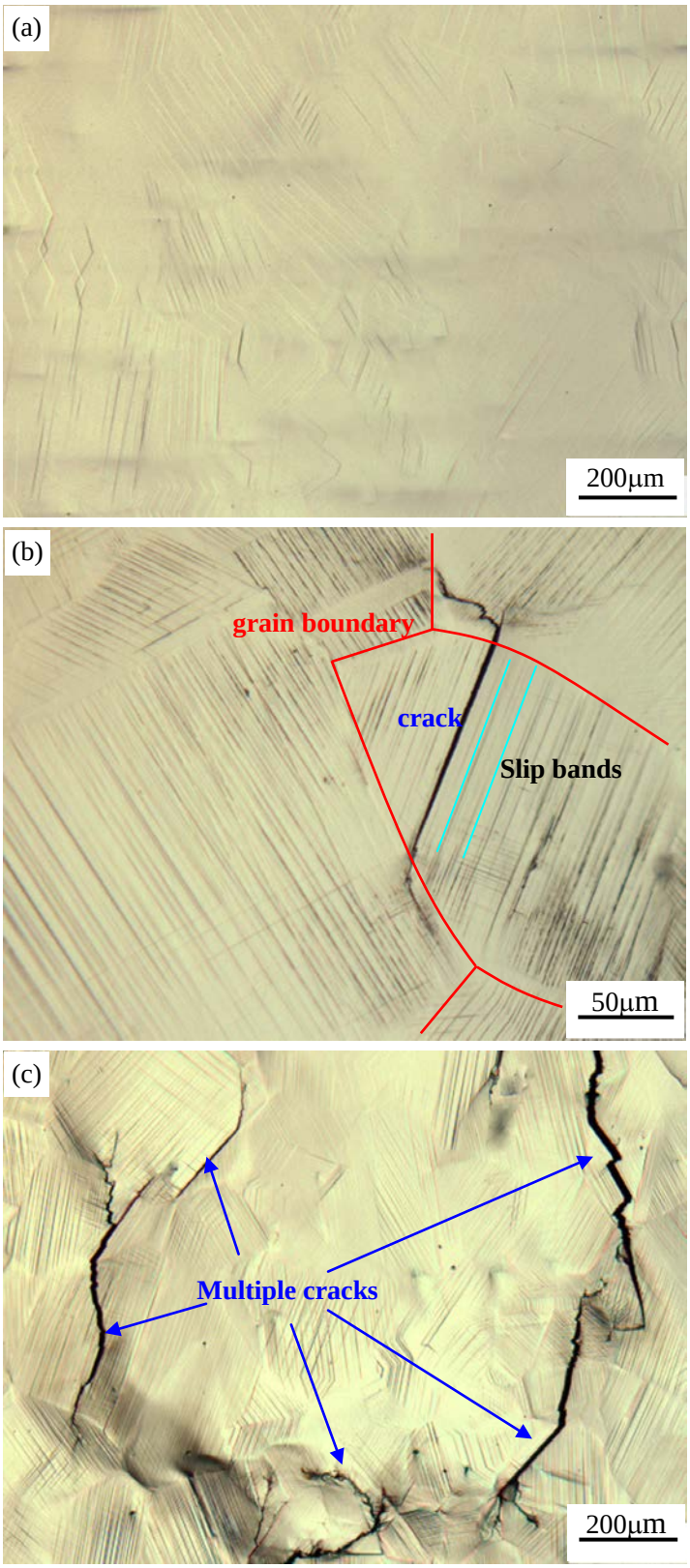

Fig.4 Surface morphology after fatigue test at different stress levels a) the maximum cyclic stress=73% σ_s, b) the maximum cyclic stress=85% σ_s, c) the maximum cyclic stress=95% σ_s

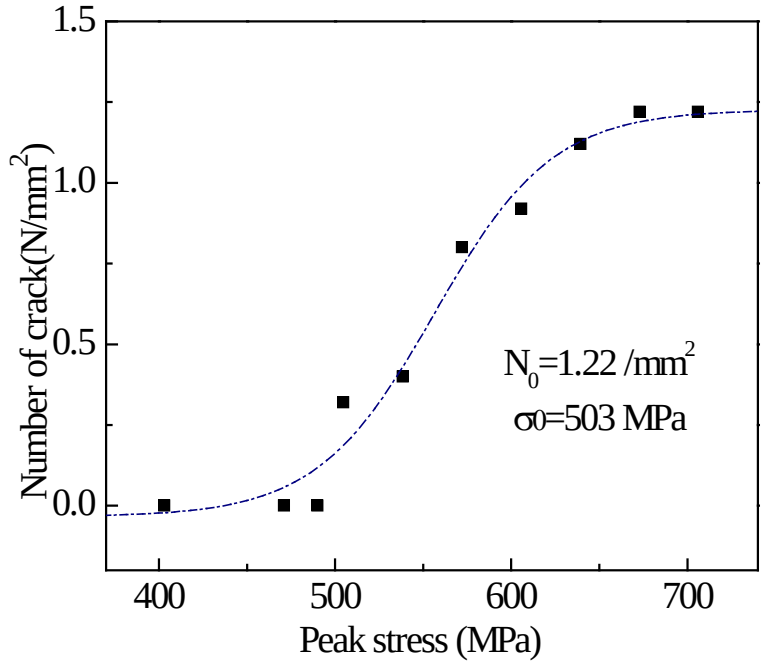

Fig.5 Plots of crack population vs applied maximum cyclic stress

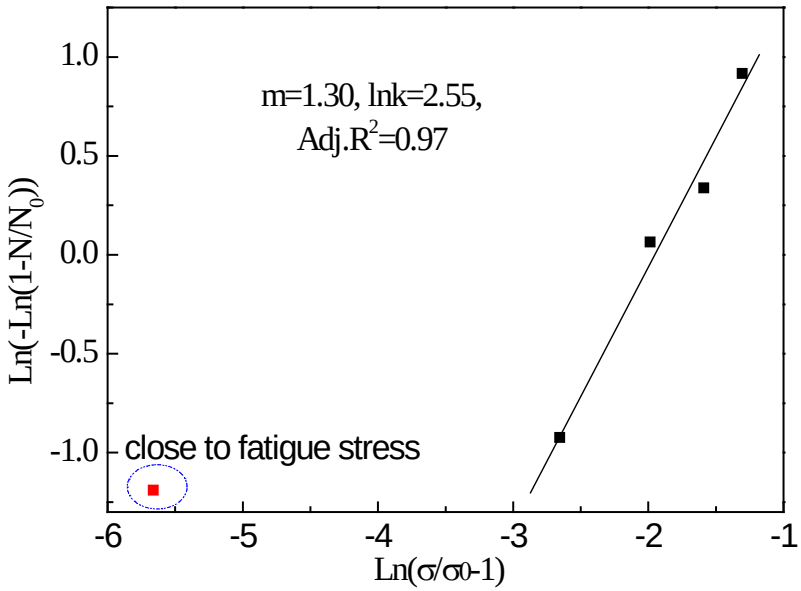

Fig.6 ln(-ln(1-(N/N_0))) vs ln ((σ/σ_0)-1) plots fitted by a Weibull function of the Cr-Mn austenite steel

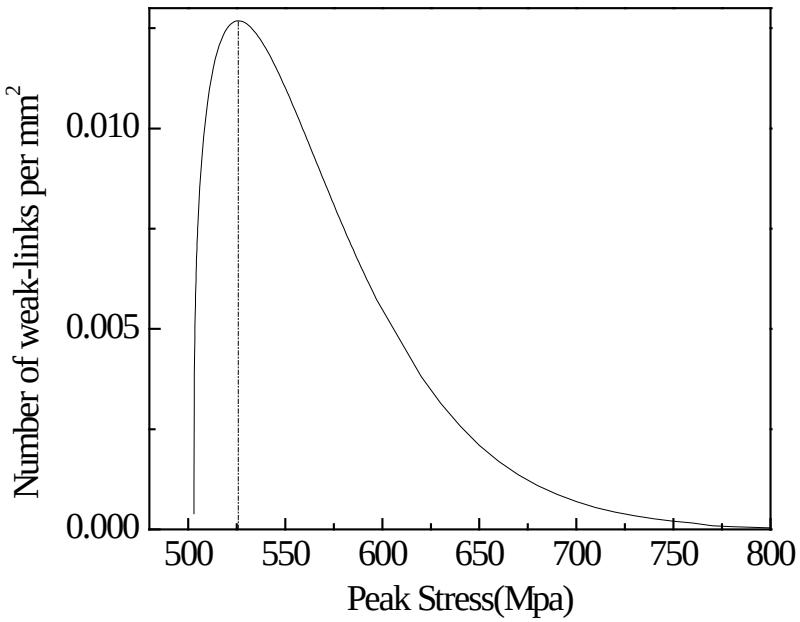

.

Fig.7 Strength distributions of fatigue weak-links of the Cr-Mn austenite steel

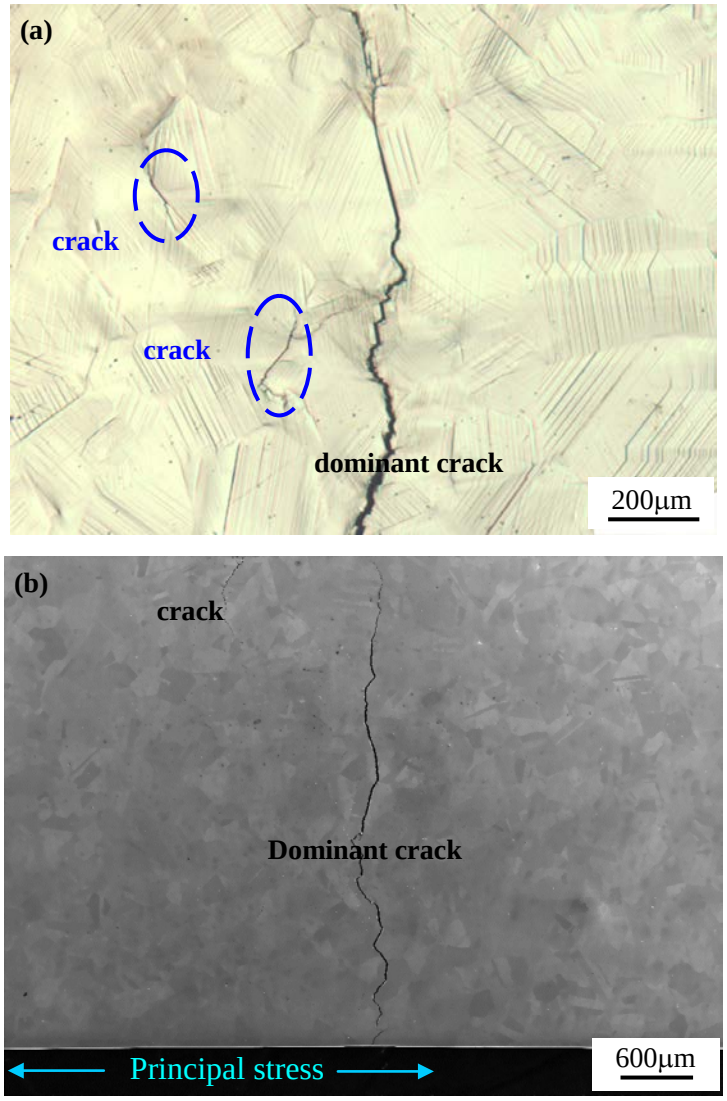

Fig. 8 The crack morphology of the fatigue sample (a) OM, 80% σ_s , (b) SEM, 90% σ_s

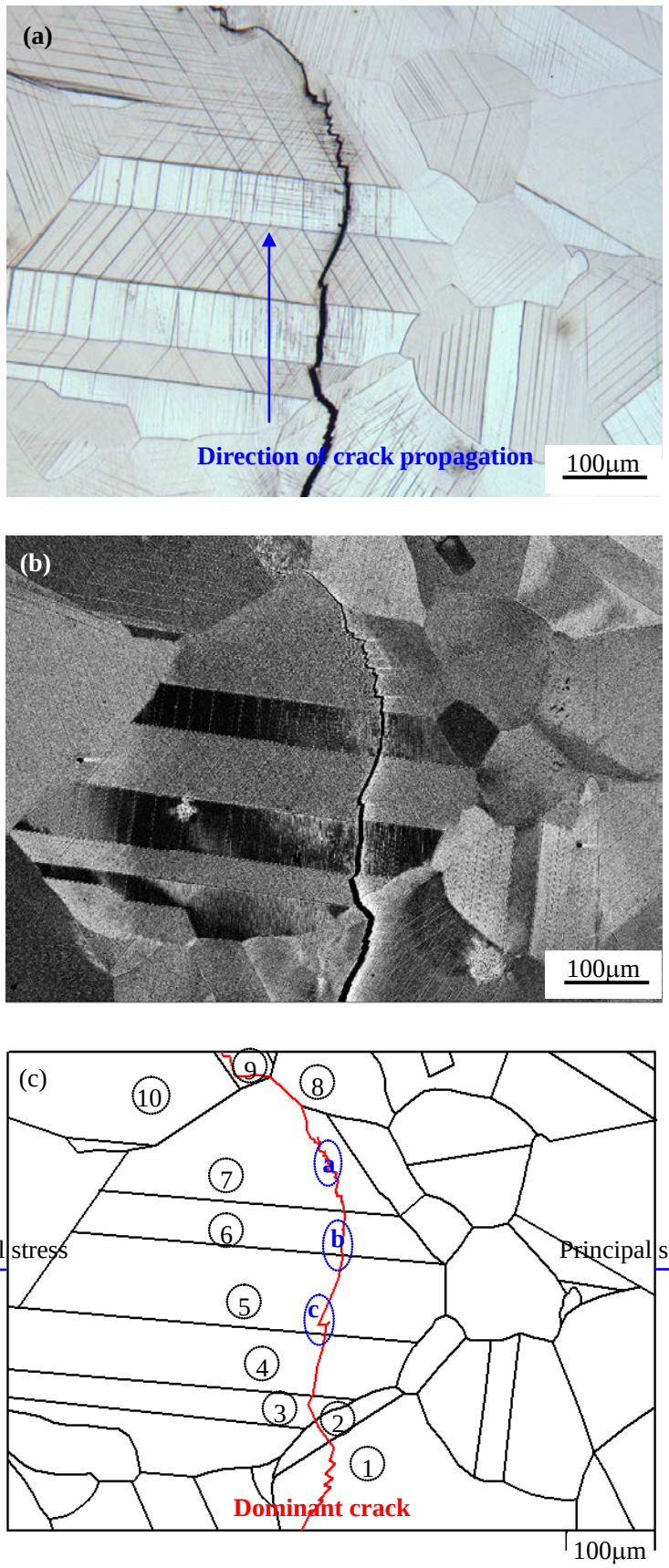

Fig. 9 A dominate crack of the fatigue sample at the stress level, 90% σ_s (a) OM (b) ECC (c) the contour lines of cracks and grains

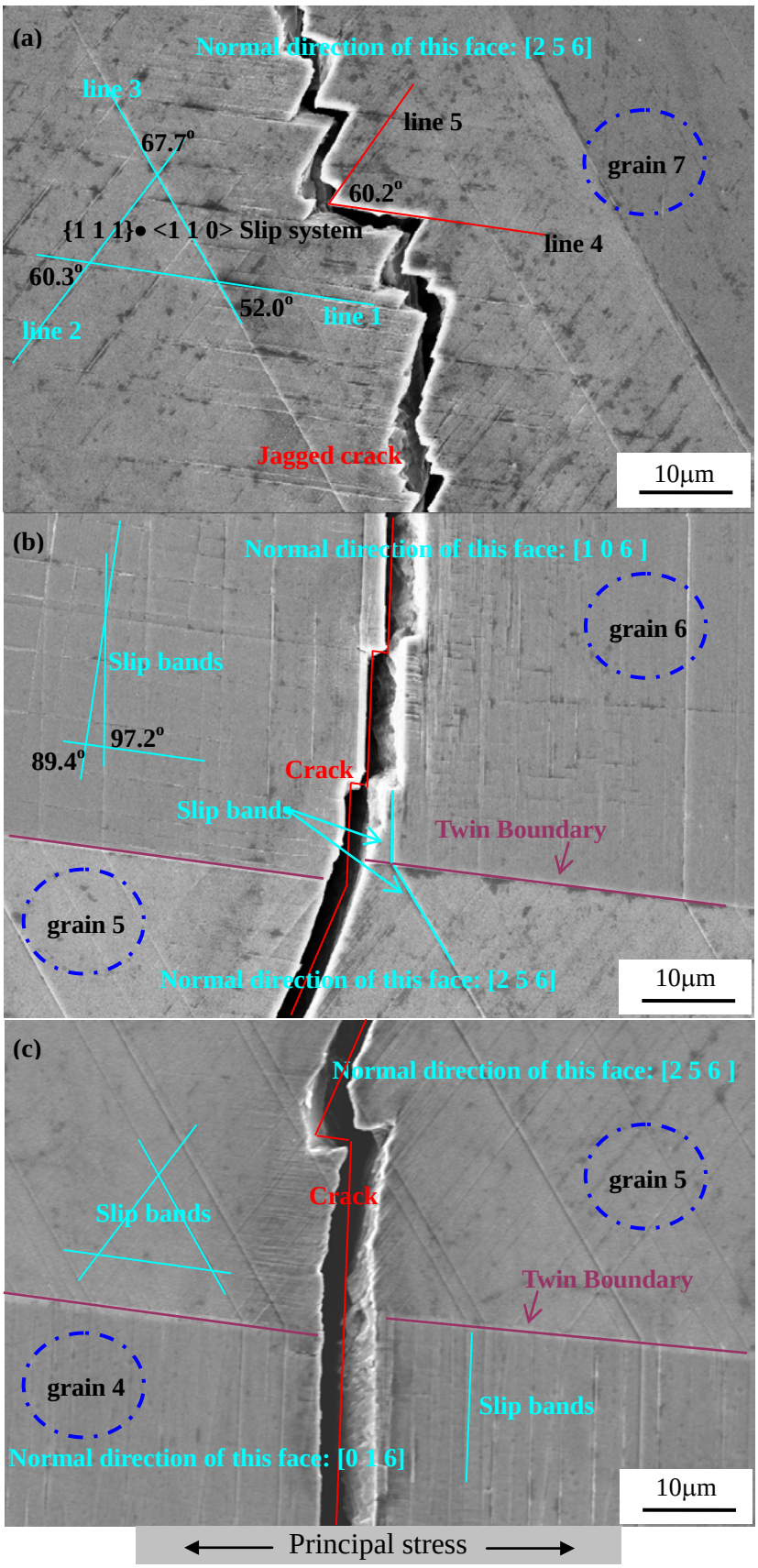

Fig10. SEM of the dominated crack for the local details corresponding to the position a, b and c in fig.9, respectively

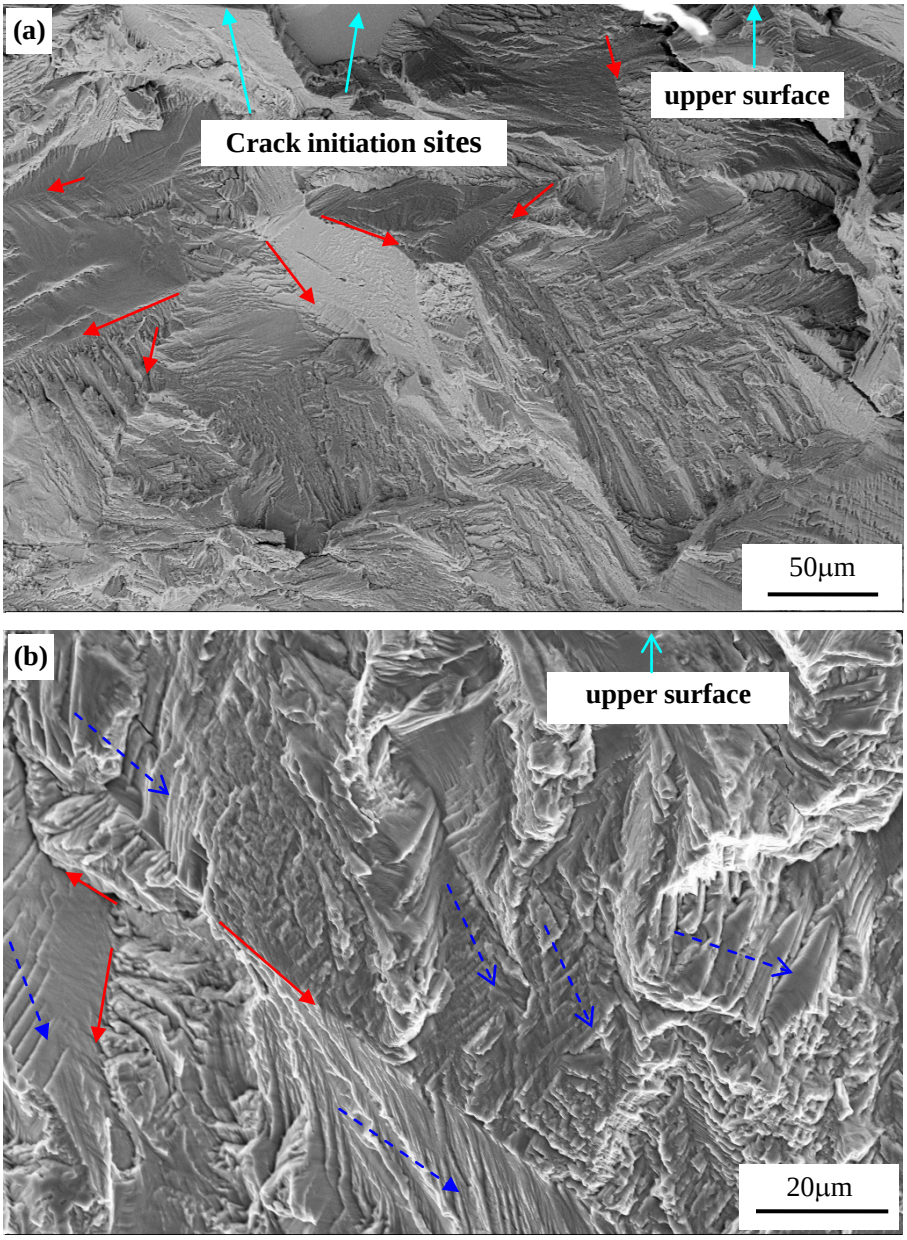

Fig11. (a) SEM micrograph of the fatigue fracture surface of an experimental steel sample, maximum stress, 100% σ_s, R=0.1, 2.7×10^5 cycles in four-point bend , (b) showing the partial details. Red arrows indicate the grain boundaries, and blue arrows show the fracture steps.

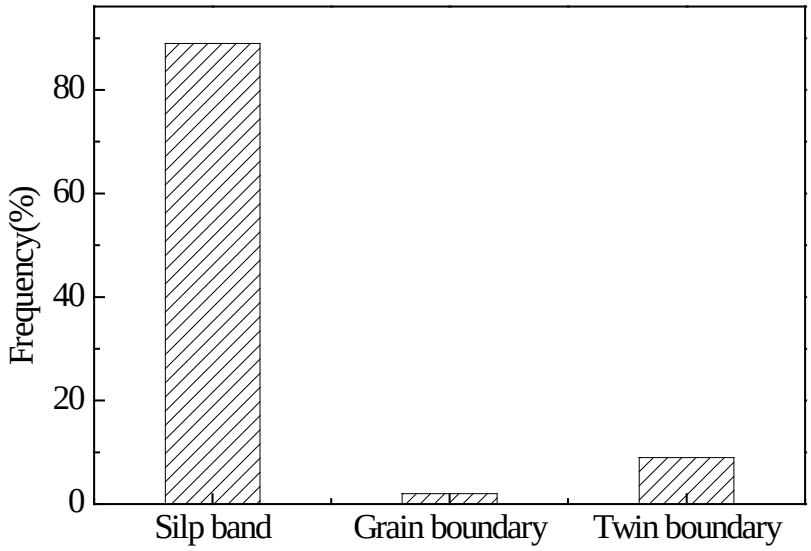

Fig. 12 Statistical data on the frequency of initiation sites

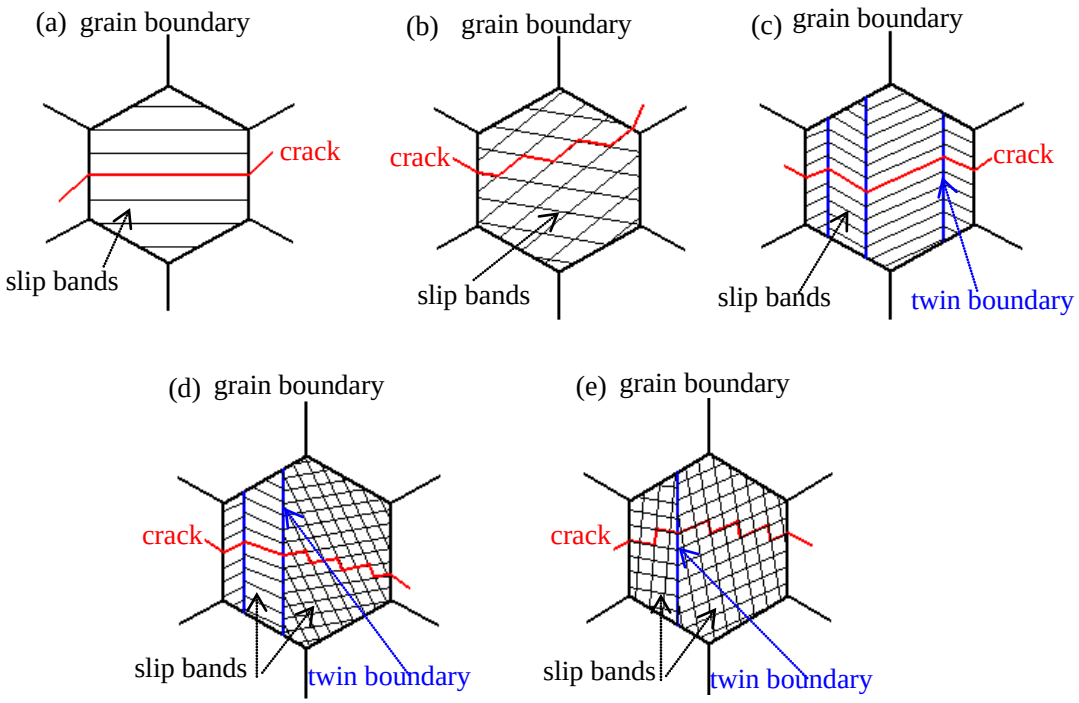

Fig.13 Schematic illustration of the propagating traces of the fatigue cracks across a grain (a) single slip (b) multiply slip (c) single slip + twinning (d) single slip + twinning+ multiply slip (e) twinning+ multiply slip